Journal of Sound and Vibration (2000) **233**(1), 137–156
doi:10.1006/jsvi.1999.2794, available online at http://www.idealibrary.com on IDEAL®

AN EFFICIENT PROCEDURE FOR VISUALIZING THE SOUND FIELD RADIATED BY VEHICLES DURING STANDARDIZED PASSBY TESTS

H. KOOK

School of Mechanical and Automotive Engineering, Kookmin University, 861-1, *Chongnung-dong, Songbuk-gu, Seoul* 136-702, *Korea*

G. B. MOEBS

Caterpillar Inc., Technical Center, Bldg. G.P.O. Box 1875, *Peoria, IL* 61656-1815, *U.S.A.*

P. DAVIES AND J. S. BOLTON

Ray W. Herrick Laboratories, School of Mechanical Engineering, Purdue University, West Lafayette, IN 47907-1077, *U.S.A.*

(*Received* 17 *May* 1999, *and in final form* 22 *November* 1999)

Throughout the world, motor vehicles are required to conform to statutory passby noise requirements. These standards usually entail the measurement of the peak A-weighted sound level while the vehicle accelerates past a stationary microphone. This pass-or-fail test is of little diagnostic value when a vehicle exceeds the statutory level. In the work presented here it is shown that a stationary array of microphones may be used to visualize the location of the noise sources on a vehicle executing a standard passby test. By locating the positions of the sources that dominate the received sideline levels, noise control efforts may be directed appropriately and efficiently. In the present work, a delay-and-sum beamformer approach was used to detect noise source locations. Algorithms have been included to correct the apparent source frequency shifts that result from the source motion. The restoration and de-Dopplerization procedure is based on using a polynomial representation of the source velocity (inferred in the first instance from a radar signal). Forward and backward propagation procedures are compared in terms of computational expense. In addition, a spherical spreading correction factor is described, along with a maximum likelihood procedure for obtaining an optimal array weighting dependent on the relative distance between the microphones and the focus point. The new weighting factor is compared with a more "intuitive" weighting factor and it will be shown that the new approach can reduce the sidelobe levels by comparison with the more intuitive approach. Experimental results presented here were based on the use of a 16 element, sparse array. It will be shown that this array could be used to identify the location and directivity of tire noise sources and of other sources on accelerating vehicles.

1. INTRODUCTION

Standardized motor vehicle passby tests are used to quantify the level of sideline noise radiated during vehicle operation [1], and governmental regulations specify the maximum A-weighted sideline sound level that is allowable. Standard vehicle passby tests make use of a single sideline microphone on each side of the vehicle to measure the peak A-weighted sound pressure level as the vehicle accelerates through a 20 m long test section

0022-460X/00/210137 + 20 $35.00/0

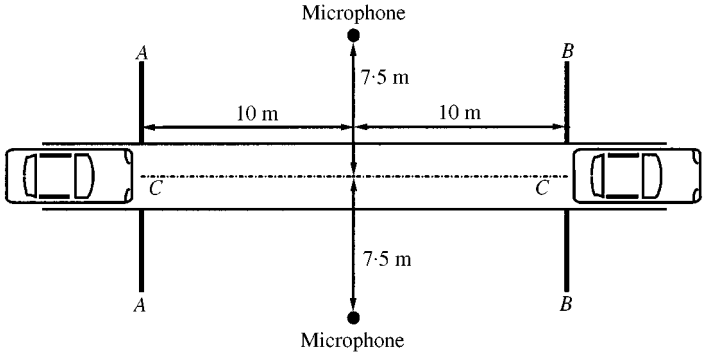

Figure 1. Standard vehicle passby tests as described in ISO 362-1981.

(see Figure 1). This pass-or-fail test has little diagnostic value when attempting to determine the reason a particular vehicle exceeds a given passby level. In the work described here, acoustical imaging techniques were used to process the output of a microphone array located to one side of the test section in order to visualize the spatial distribution of noise sources on a moving vehicle. It is suggested that these acoustical imaging techniques could be used to supplement standard passby measurements: the information they yield allows the location of the predominant noise sources to be identified, thus indicating where noise control resources should be directed. Note that the work described here is a direct extension of the work presented earlier [2].

Microphone arrays have proven to be useful for identifying noise sources on moving as well as on stationary sources [3]. The so-called spherical beamforming is typically used when the microphone array is located relatively close to the source [4], while planar beamforming [5] is used when the microphone array is located far enough from the source such that the paths from the source to each of the array elements are approximately parallel. Many types of array configurations have been used in the past. Among them are linear arrays [6], regular two-dimensional arrays [7], non-redundant arrays [8] and crossed arrays [9]. Non-uniform array configurations have been used to reduce the amount of redundant information gathered by the array at the expense of increasing sidelobe levels in the array directivity pattern [10]. It has also been shown that sidelobe levels can be reduced by applying appropriate spatial windows to the outputs of the microphones comprising the array [4]. In addition, array outputs can be processed either in the frequency or in the time domains [10].

In the approach described here, the sound field generated by a moving vehicle was measured by using a stationary array of microphones located relatively close to, and parallel with, the vehicle track. The array configuration was random and two-dimensionally sparse, and the microphone outputs were processed in the time domain. When the array element signals were summed, the focus of the beamformer was arranged to be at an assumed source location fixed with respect to a "reconstruction" plane close to, and moving with, the vehicle. A sketch of the stationary array of microphones and reconstruction plane attached to one side of the moving vehicle is provided in Figure 2. By reconstructing the sound field at a sequence of points on the reconstruction plane, the source strength distribution can be obtained at any instant during the passby test.

When performing spherical beamforming, weighting factors that depend on the time-varying propagation distances are applied to the output of each microphone. These weights compensate for the pressure attenuation due to spherical spreading and "restore"

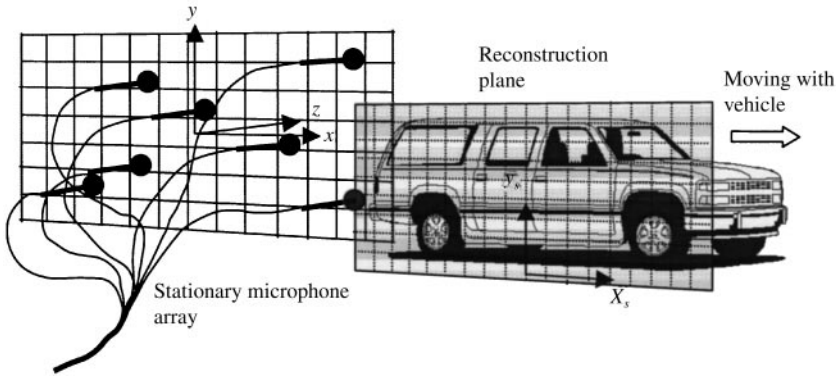

Figure 2. Beamforming on a reconstruction plane attached to and moving with the vehicle.

the estimates of the vehicle source strength to the grid points on the reconstruction plane. In the present paper, a new method for formulating the weighting factors applied to each microphone has been developed based upon the maximum likelihood estimation technique and its performance is compared with a more intuitive approach.

2. DE-DOPPLERIZATION PROCEDURE

In the experiments reported here, an array of microphones placed 7·5 m from, and parallel with, the test section centerline received spherically attenuated and Doppler-shifted signals from the vehicle while the latter executed a conventional passby test. The attenuation results from the spherical spreading that occurs during the propagation from the source point to the array, and the Doppler frequency shift results from the source motion with respect to the fixed receiver array. In order to recreate the source strength distribution on a surface in the moving source frame of reference, signals received by each microphone must be de-Dopplerized and their amplitudes corrected before they are summed to yield an estimated source strength at the specific grid point on the reconstruction plane. The key parameter in both the amplitude correction and the de-Dopplerization operations is the propagation distance from the source to each of the array microphones at each sample time. Thus, propagation distance must be calculated for each combination of a stationary array microphone and a grid point on the moving reconstruction plane. Those distances can be calculated when the source motion is known as a function of time, and when the array location with respect to the vehicle track is specified. To identify the source strength at a particular grid point on the reconstruction plane, either "forward propagation" or "backward propagation" calculation procedures can be used. Each of these procedures will be discussed below, but first the representation of the vehicle motion will be described.

2.1. VELOCITY PARAMETRIZATION

In Figure 3, a typical velocity profile for a passenger vehicle during a passby event is shown: this profile was created by processing a radar signal. The vehicle enters the test section slightly before 4 s, and exits the test section shortly after 5 s. Note that the apparently large fluctuations in vehicle velocity (e.g., near 1, 2·8 and 4 s) occur because of

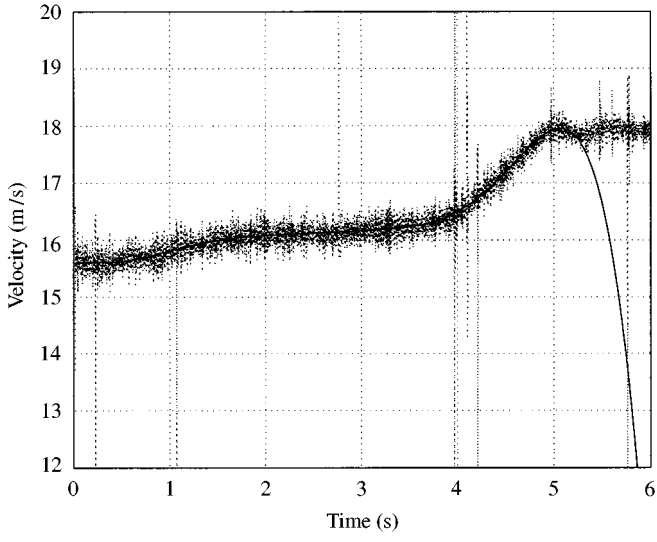

Figure 3. Typical velocity profile during a normal passby test: measured velocity data (····) and polynomial fit (——).

"drop out" of the radar signal. As shown in Figure 3, an *n*th order polynomial can be fitted to the instantaneous velocity curve. A polynomial representation of the vehicle velocity is very useful for three reasons: (1) the effect of noise in the velocity estimation procedure is reduced and the velocity profile is smoothed, resulting in a good representation of the vehicle motion (whose actual velocity fluctuations are limited by the vehicle's inertia); (2) the radar signal dropouts, which result in poor or zero velocity estimates in particular time segments, can be ignored in the curve fitting; and (3) in the backward propagation calculation, which will be described later, the polynomial representation allows the propagation distance between source and receiver to be calculated numerically to any desired level of accuracy (given that the absolute vehicle position is known at one instant), a procedure that is also efficient since the derivative of the propagation distance with respect to time can be found in closed form from the velocity polynomial. The latter point is particularly important since a knowledge of the derivative of the propagation distance and a function of the vehicle velocity, is required to perform an efficient iterative solution for the propagation distance which is a part of the backward propagation calculation.

2.2. FORWARD PROPAGATION VERSUS BACKWARD PROPAGATION

Since the distances between the source reconstruction positions and the array microphones are continually changing due to the source motion during the test, microphone signals sampled at equally spaced times were not emitted at equally spaced times; acoustical signals received at the same sample time at two different microphones are usually emitted by the source at different times. To be able to sum the "restored" output of each microphone in the vehicle frame of reference on the restoration plane and to perform frequency analysis by using conventional fast Fourier transforms (FFTs), the microphone outputs must be processed to yield equally spaced time histories for a point on the reconstruction plane. The propagation distances must be known in order to obtain uniformly sampled signals in the source time frame, so that the sampling times are the same

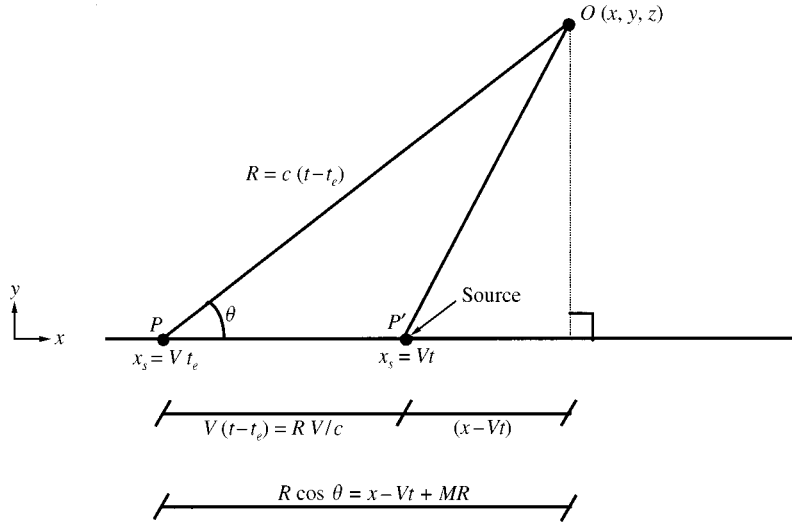

Figure 4. Kinematics of radiation from a source moving in a straight line and at a constant velocity.

for each receiver. In the present study, both backward and forward propagation procedures for performing this operation were implemented for comparison.

The kinematics of sound radiation from a source moving in a straight line with respect to a stationary microphone is illustrated in Figure 4. In the figure, the source is shown moving at a constant velocity, V, from left to right (in the positive x direction) while radiating sound. The points P and P′ represent the positions of the source, (x_s, y_s, z_s), at times t_e and t respectively. A microphone positioned at the point, O(x, y, z), receives a signal at time t (which is here equivalent to the so-called receiver time, t_r) which was emitted from the source at the emission time t_e. Note that the propagation distance of the signal received by the microphone at time t is $\overline{\mathrm{OP}}$ (also denoted as R in the figure). Then it is not difficult to obtain an explicit expression for the propagation distance, R, for the signal received at time t, i.e.,

$$R = \frac{M(x - Vt) + \sqrt{(x - Vt)^2 + (1 - M^2)(y^2 + z^2)}}{1 - M^2}, \tag{1}$$

where M is the Mach number of the source. For a vehicle undergoing arbitrary acceleration, Equation (1) can be used only to produce an initial guess of the propagation distance, R; more accurate values of R can be obtained by solving a generalized equation based on a knowledge of the source position as a function of time, i.e.,

$$R^2(t_r) = [x - x_s(t_e)]^2 + [y - y_s(t_e)]^2 + [z - z_s(t_e)]^2. \tag{2}$$

since equation (2) is not explicit in R (because $t_e = t_r - R(t_r)/c$), it must be solved by using an iterative method which in the present case was based on using a polynomial representation of the vehicle velocity as a function of time.

The procedure for transforming the sampled signals received at each microphone into restored signals at a focus point on the reconstruction plane which are regularly sampled with respect to the emission time vector is illustrated in Figure 5 and it can be summarized as follows:

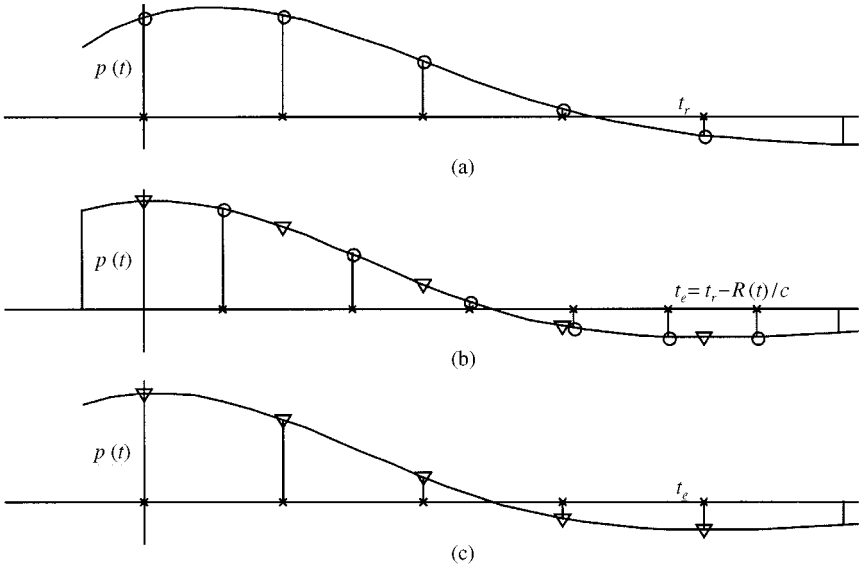

Figure 5. Illustration of the sequence of operations for the backward propagation method: (a) samples received at equally spaced time vector, t_r; (b) dilation of the samples (circles) using non-equi-spaced emission time vector, t_e and resampled data (triangles) using an equally spaced time vector, t_e; (c) resulting equi-spaced samples.

Given a point on the reconstruction plane, repeat for each receiver microphone:

1. *Calculate the propagation distance,* $R(t_r)$*, for the samples received at* t_r *(receiver time).*
2. *Generate the emission time vector corresponding to the receiver times by using the formula,* $t_e = t_r - R(t_r)/c$*, the result being a non-equi-spaced time vector (from, Figure* 5(*a*) *to* 5(*b*)).
3. *Each sample of the received signal is identified with a particular emission time, and the resulting non-equi-spaced time history is resampled to obtain an equally spaced time history in the source (i.e., emission) time frame (from Figure* 5(*b*) *to* 5(*c*)).

Continue

To reduce the computational load entailed by Step 1, the propagation distance can be calculated at every *n*th sample, the propagation distances for all the skipped samples being obtained by interpolation. To verify that this approach is computationally accurate, the propagation distance for a pair comprising a microphone and a grid point was obtained both by calculating a result for every point in the receiver time vector and by calculating a result at every 500th point with the skipped samples being obtained by interpolation. The results obtained using each method are compared in Figure 6(a), and as can be seen, these two curves coincide within the width of the curve. The numerical deviation of the curve obtained by using the latter method was normalized by the tolerance value (10^{-3} m) used in the iteration procedure and is represented in Figure 6(b). As can be seen in the figure, this method is both feasible and accurate since the propagation distance is a smooth function of time.

In the work reported in reference [2, 11], a cubic spline interpolation was used for both the propagation distance interpolation in Step 1, and for the temporal resampling in Step 3. A subsequent computation time analysis showed that Steps 1 and 3 consumed approximately 32 and 42%, respectively, of the total computational time required by the reconstruction process. That is, cubic spline interpolation procedures accounted for almost three-quarters of the total computation time when using the backward propagation

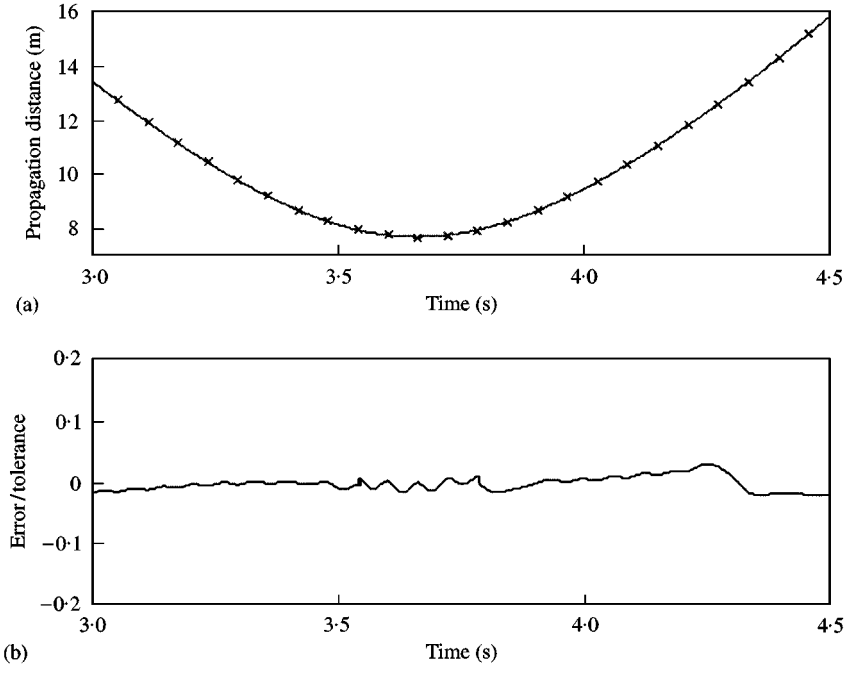

Figure 6. The propagation distance between a microphone and a grid point as a function of time; the velocity profile represented in Figure 3 was used in the calculation: (a) the curve evaluated at all the points in the receiver time vector and the curve obtained by spline-interpolating the points evaluated at every 500 points (X's) coincide within the width of a single curve; (b) the deviation of the latter curve from the former one was normalized using the tolerance value (10^{-3} m) used in the iteration procedure for the propagation distance calculation.

procedure. This observation prompted the development of an alternative process, here referred to as the forward propagation procedure.

In the forward propagation procedure (see Figure 7), the propagation distance is first calculated for a signal emitted at equally spaced emission times, t_e, thus making the cubic spline interpolation unnecessary [12], i.e.,

Given a point on the reconstruction plane, repeat for each receiver microphone:

1. *Calculate the instantaneous distance, $D(t_e)$, between the assumed source position and the microphone for an assumed signal emitted at t_e (emission time).*
2. *Generate the corresponding receiver time vector by using the formula, $t_r = t_e + D(t_e)/c$. The measured microphone outputs sampled at equally spaced sample times in the receiver time frame are resampled using the unevenly spaced receiver time vector (from Figure 7(a) to 7(b)).*
3. *The resulting samples are then signals emitted at equally spaced time in the source time frame (from Figure 7(b) to 7(c)).*

Continue

The instantaneous distance function, $D(t_e)$, is different from the propagation distance function, $R(t_r)$, and it can be related to the propagation distance function through the relation $D(t_e) = R(t_e + D(t_e)/c)$. The instantaneous distance calculation, i.e., Step 1 in the latter procedure, is straightforward: that is, $D^2(t_e) = [x - x_s(t_e)]^2 + [y - y_s(t_e)]^2 + [z - z_s(t_e)]^2$, where (x, y, z) and (x_s, y_s, z_s) represent the positions of a microphone and the

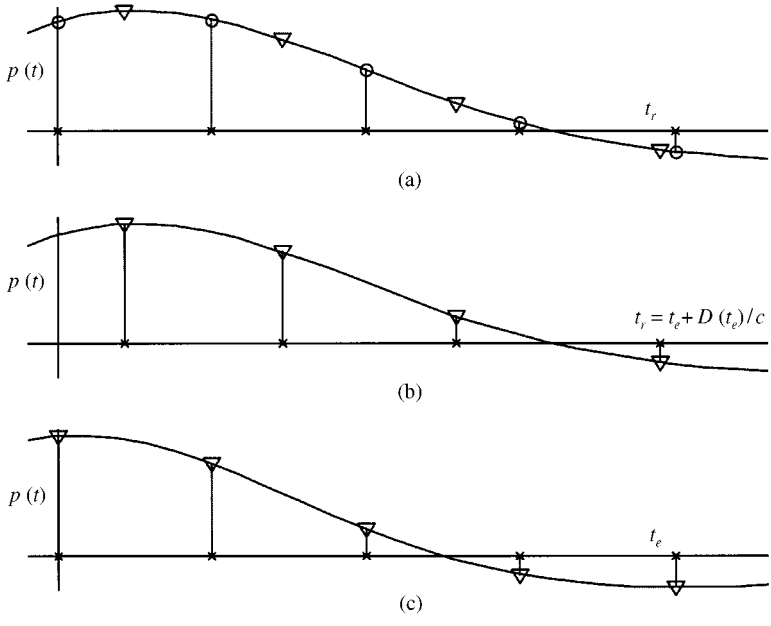

Figure 7. Illustration of the sequence of operations for the forward propagation method: (a) samples received at equally spaced time vector, t_r (circles) and resampled data (triangles) using non-equi-spaced receiver time vector, t_r; (b) resulting data; (c) equally spaced samples after dilation.

grid point on the reconstruction plane respectively. Given the position of a grid point on the restoration plane (i.e., an assumed source location) as a function of emission time, the propagation distance to a specific receiver is simply the instantaneous distance between the grid point and the receiver at that time. Step 2 results in an unevenly spaced receiver time vector, which does not necessarily coincide with the sampling points in the measured microphone outputs. Thus, the signals that were emitted at the emission time, t_e, towards each of the array microphones can be obtained in Step 3 by interpolation: in the procedure implemented in the present work, a linear interpolation was used to perform this step instead of the cubic spline interpolation used earlier [2], since the time history consists of relatively densely spaced samples. While linear interpolation is not highly accurate, the noise added to the microphone signals in this process does not appear to be more significant than that created by the other elements of the complete restoration process. The sample rate used in the measurements presented here was 8192 Hz, and the low-pass anti-aliasing filters were set at 3200 Hz. The use of higher sample rates would of course reduce the linear interpolation error [12].

3. AMPLITUDE ESTIMATION

After the signals from each microphone sensor are time-delayed, and shifted to remove the Doppler effect and to focus the array on a particular reconstruction point, they must be multiplied by appropriate weighting factors, w_{ij}, to account for spherical spreading before they are summed. When the array is focused on the jth grid point on the reconstruction plane, the array outputs, $z_j(t)$, can thus be represented as

$$z_j(t) = \sum_{i=0}^{M-1} w_{ij} y_i(t + R_{ij}/c), \tag{3}$$

where $y_i(t)$ represents the signal received by the ith microphone at time t, and R_{ij} denotes the propagation distance of a signal emitted at the jth grid point and received by the ith microphone sensor at time t.

Since the pressure received at the ith microphone is inversely proportional to the propagation distance, R_{ij}, an intuitively appealing weighting factor is simply R_{ij}, since it would appear to eliminate exactly the attenuation due to spherical spreading. Nonetheless, it transpires that this weighting factor is not generally optimal in terms of sidelobe levels. In this section, the development of an improved weighting factor is described.

3.1. MAXIMUM LIKELIHOOD ESTIMATION

Maximum likelihood estimation is one of the most popular methods for estimating the value of unknown parameters based on the observation vector of one or more signals. It is well known that conventional planar (i.e., far field) beamforming method yields maximum likelihood estimates of the amplitude of a single monopole source when the background noise is spatially white [10] and when unit weighting is given to each sensor output. In the work described in this subsection, a weighting factor that yields the maximum likelihood estimate of the amplitude of a single nearfield source when using the spherical beamforming method was identified.

Consider signals that are emitted by a single source located in the near field: the position vector of the source is denoted by $\mathbf{R}^0$, with the origin being at the phase center of the microphone array (i.e., at the geometrical center of the microphone array). For a moving source, the ith sensor signal, $y_i(t)$ can be represented as

$$y_i(t) = \frac{1}{R_i^0 |1 - M_r^i|} a\left(t - \frac{R_i^0}{c}\right) + n_i(t), \tag{4}$$

where $a(t)$ is the source signal at time t, R_i^0 is the propagation distance of the signals received by the ith microphone at time t, R_i^0/c represents the time delay corresponding to the propagation time from the source to the ith microphone, M_r^i denotes the component of the source Mach number in the direction of the ith microphone at emission time $t_e = t - R_i^0/c$, and $n_i(t)$ is uncorrelated background noise at the ith microphone location.

Note that in equation (4), the effect of ground reflection is not considered explicitly. The ground reflection effect, however, can be represented by the contributions of image sources placed in the free field. For an ideal case of an array aperture function with a narrow mainlobe and low sidelobe levels that is focused at a point above ground, signals reflected from the ground surface, i.e., which appear to originate at image sources below ground level, would cancel out perfectly unless the source was located at ground level. In practical cases, when the array aperture function is such that the rejection of the contributions from sources located some distance from the focused point is incomplete, there is leakage from the image source into the "real" source: this effect causes the amplitudes of source near ground level to be overestimated (since both the real and image sources may fall within the mainlobe of the array aperture function). Note however that ground level sources are not, in principle affected, since the real sources and image sources coalesce in this case (and in the case of tire noise, for example, it is presumably of interest to know the source contributions in the presence of the ground rather than under free space conditions). In the present paper, it is assumed that microphone arrays have reasonably good sidelobe rejection (which is an underlying assumption in delay and sum beamformer approach, generally), and no specific account has been taken for ground effects: explicit consideration of the latter will be saved for future work.

To begin with, only the signal's waveform, $a(t)$, is assumed to be unknown while the position of the source, R_i^0 (i.e., a particular candidate source location on the reconstruction lane) is assumed to be known. When vectors, $\mathbf{y}$, $\mathbf{s}$, and $\mathbf{n}$ are defined as

$$\mathbf{y} = \{y_0(t + R_0^0/c), y_1(t + R_1^0/c), \ldots, y_{M-1}(t + R_{M-1}^0/c)\}^{\mathrm{T}},$$

$$\mathbf{s} = \left\{\frac{1}{R_0^0|1 - M_r^0|}, \frac{1}{R_1^0|1 - M_r^1|}, \cdots, \frac{1}{R_{M-1}^0|1 - M_r^{M-1}|}\right\}^{\mathrm{T}},$$

$$\mathbf{n} = \{n_0, n_1, \ldots, n_{M-1}\}^{\mathrm{T}}, \tag{5}$$

then, a single observation vector of the delayed signals from the array can be written as

$$\mathbf{y} = a(t)\mathbf{s} + \mathbf{n}. \tag{6}$$

After assuming the background noise to be Gaussian, to be stationary with respect to time and position, and to have a known covariance matrix, $\mathbf{K_n}$, the logarithm of the observation vector's joint probability density function can be represented as [10]

$$\ln p_{\mathbf{y}|a(t)} = -\tfrac{1}{2}\ln\det[2\pi\mathbf{K_n}] - \tfrac{1}{2}[\mathbf{y} - a\mathbf{s}]'\mathbf{K_n}^{-1}[\mathbf{y} - a\mathbf{s}]. \tag{7}$$

A conditional probability density function, $p_{E1/E2}$, denotes the probability density of event $E1$ occurring when event $E2$ has already occurred. Therefore, $p_{\mathbf{y}/a}$ denotes the joint probability density of the vector $\mathbf{y}$ being observed when the signal source amplitude was $a(t)$ at time t which corresponds to the location, $\mathbf{R}_0$.

The maximum likelihood estimate of $a(t)$ is the value of the parameter, a, that will maximize the value of equation (7); it can thus be found as the solution of

$$\min_a [\mathbf{y} - a\mathbf{s}]'\mathbf{K_n}^{-1}[\mathbf{y} - a\mathbf{s}], \tag{8}$$

where $[\ ]'$ represents the complex conjugate transpose (i.e., the Hermitian transpose) of a complex vector. The minimum of the last expression is found by evaluating its derivative with respect to the parameter a, setting the result to zero, and solving, i.e.,

$$a: \ -\mathbf{s}\mathbf{K_n}^{-1}(\mathbf{y} - a\mathbf{s}) = 0. \tag{9}$$

The maximum likelihood estimate of the amplitude, $\hat{a}_{ML}$, can therefore be written from equation (9) as

$$\hat{a}_{ML} = \mathbf{s}'\mathbf{K_n}^{-1}\mathbf{y}/\mathbf{s}'\mathbf{K_n}^{-1}\mathbf{s}. \tag{10}$$

When the special case of spatially white background noise is considered, the noise covariance matrix is proportional to the identity matrix, and the amplitude estimate $\hat{a}_{ML}$ becomes

$$\hat{a}_{ML} = \mathbf{s}'\mathbf{y}/\mathbf{s}'\mathbf{s} \tag{11}$$

or equivalently,

$$\hat{a}_{ML}(t) = \frac{\sum_{i=0}^{M-1} y_i(t + R_i^0/c)/R_i^0|1 - M_r^i|}{\sum_{i=0}^{M-1} 1/(R_i^0|1 - M_r^i|)^2}. \tag{12}$$

Recall that the source position vector, $\mathbf{R}^0$, and thus R_i^0 in equation (12) are assumed to be known. When the present maximum likelihood estimation method is to be used in combination with a spherical beamforming method, it is assumed that a source is positioned at the jth grid point each time the array is focused on that grid point, and that, therefore, the source position is "known". This means that R_i^0 in equation (12) should be replaced by R_{ij} (note that the dependence of M_r on R_{ij} has not been expressed explicitly in equation (12)).

When equation (12), with R_i^0 replaced by R_{ij}, is used to sweep the assumed position vector over the reconstruction grid points, the resulting amplitude estimates, a, in equation (11) can be interpreted as the amplitude estimate of the source at the assumed position at time t. Therefore the vector, $a\mathbf{s}$ in equation (8) represents the signals which are predicted to reach each microphone at time t plus the propagation delay time which is different for each microphone. Since the vector $\mathbf{y}$ denotes the measured signals at each of the microphones at the corresponding times, the quantity $\mathbf{y} - a\mathbf{s}$ in equation (8) denotes the discrepancies between the measured and predicted signals at each microphone, i.e., it is the vector of the error signals. Therefore, equation (8) can be interpreted as the sum of the squared amplitudes of the errors at each microphone for the estimated source strength at time t (which has the dimension of power).

When the Mach number is assumed to be small, which is the case for usual motor vehicle passby tests, the effects of Mach number can be considered negligible [11], thus the weighting factor for the maximum likelihood amplitude estimation can be simplified and identified by comparison of equation (12) with equation (3), i.e.,

$$w_{ij} = \frac{1/R_{ij}}{\sum_{i=0}^{M-1} 1/R_{ij}^2}. \tag{13}$$

Note that the weighting factor has the same dimension as R_{ij}. Therefore, when the weighting factor represented by equation (13) is applied to the spherical beamforming case, it yields the maximum likelihood amplitude estimate at the true source position for the case of a single monopole source with spatially white background noise.

Figure 8 shows simulated results that allow a comparison of the intuitively "correct" weighting factor, R_{ij}, and the maximum likelihood amplitude correction factor given by equation (13). A stationary unit amplitude source radiating a 500 Hz pure tone was assumed to be positioned 7·5 m from the phase center of the array in the y-direction (i.e., $x = 0$ m and $y = 7{\cdot}5$ m). The receiver array used was a uniformly spaced horizontal linear array with an interesting separation of 50 cm. The restored power distribution over the interval $-2{\cdot}0$–$2{\cdot}0$ m obtained by using a linear array composed of 16 microphones is shown in Figure 8(a). The use of the new weighting factor defined in equation (13) slightly widened the main lobe, while decreasing the sidelobe levels. The sidelobe level reduction is more easily seen in Figure 8(b), in which case the number of microphones was increased from 16 to 64 at the same intersensor separation. As shown in Figure 8(b), when the weighting factor, R_{ij}, was used, the level of the first sidelobe was about 5 dB below the main lobe. When the new weighting factor was used, the sidelobe level was more than 10 dB below the main lobe. A similar reduction in sidelobe level was observed when the new weighting factor was applied to an array in which the intersensor spacing was increased while maintaining the same number of microphone instead of increasing the number of

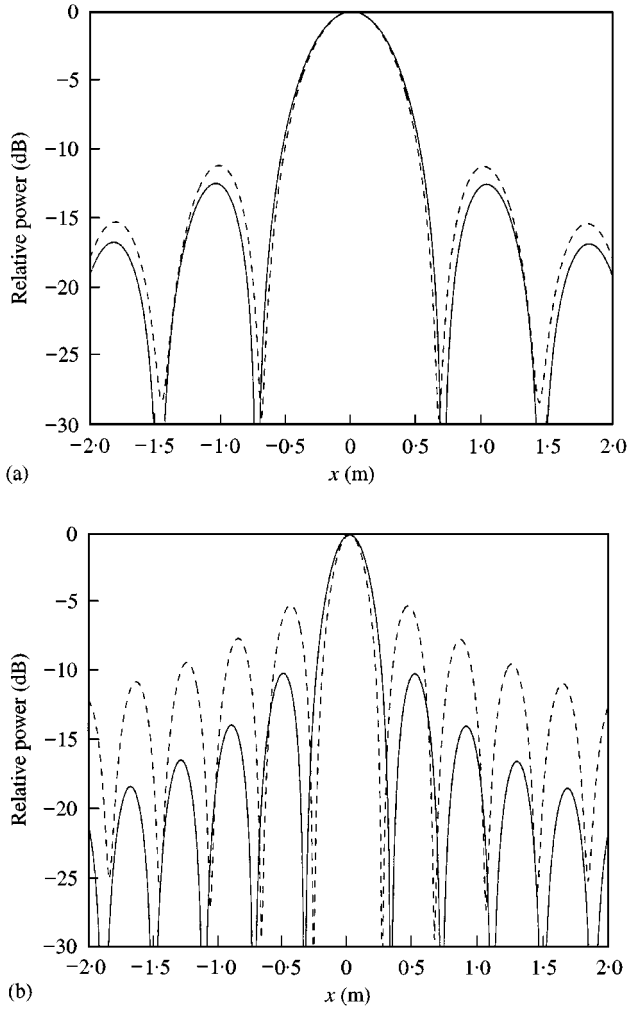

Figure 8. Comparison of the directional patterns associated with two beamformer weighting factors. Source frequency, $f = 500$ Hz, source position $x_0 = 0$. Solid line: weighting factor, equation (13). Dashed line: weighting factor, R_{ij}. (a) 16-microphone array; (b) 64-microphone array.

sensors at a constant intersensor spacing (as in the example discussed above). Thus, it can be concluded that the total aperture size determines the sidelobe level reduction.

3.2. SOURCE LOCATION ESTIMATES

When the array is focused on an assumed source position (i.e., $\mathbf{R}_{ij} = \mathbf{R}_i^0$), the source strength estimate given by equation (12) is the true source amplitude, a, and that value causes equation (7) to be maximized (when the source is a monopole). In the case of planar beamforming, in which case unity weighting values are applied to each microphone output, the estimated source strength at the true source position is again the maximum value evaluated on the reconstruction plane. Thus, the source position in the single source case can be easily identified as the location of the peak on the reconstruction plane.

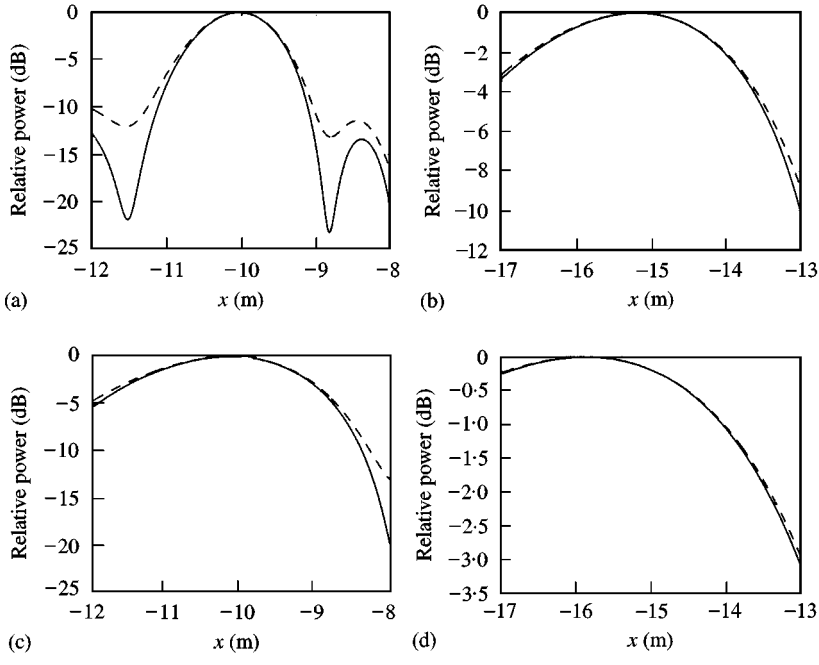

Figure 9. Apparent shift of source location. Weighting factor R_{ij} (dashed line); weighting factor of equation (13) (solid line); (a) $f = 1000$ Hz, $x_0 = -10$ m; (b) $f = 1000$ Hz, $x_0 = -15$ m; (c) $f = 500$ Hz, $x_0 = -10$ m; (d) $f = 500$ Hz, $x_0 = -15$ m.

However, the maximum of the restored source strength distribution on the reconstruction plane may not coincide with the true source location when spherical beamforming is performed. This effect is true even though the source strength evaluated at the true source position has its correct value and even though the likelihood function in equation (7) yields its maximum value at that position for the case of the single monopole source.

Figure 9 shows simulated results obtained when it was assumed that the signal source was positioned to one side of the phase center of the equally spaced linear array, i.e., towards one end of the test section. It can be seen that the peak is offset from the true source location, especially as the frequency decreases [see Figure 9(d)]. The ability of the focused array to resolve the source position thus diminishes when the source is offset from the phase center of the array, and this is true for both sets of weighting factors considered here.

As noted, the error in resolving the source position increases as the distance between the source and the phase center ($x = 0$) increases in the x direction (see Figures 9(a) and 9(b) for 500 Hz source case, and Figures 9(c) and 9(d) for a 1000 Hz source case). Note that the angle between the "look"-direction and the reconstruction plane becomes acute as the reconstruction plane is moved away from the phase center of the array. As the reconstruction plane becomes increasingly parallel with the look-direction, source strengths at neighboring grid points in the x directions effectively coalesce in the look-direction. The apparent broadening of the source occurs since constructive and/or destructive interference among the delayed microphone outputs does not work as well in the radial direction (i.e., in the look-direction) as in the direction perpendicular to the radial direction. That is, the amplification resulting from application of the correction factors associated with the grid points on the far side of the source position exceed the attenuation resulting from

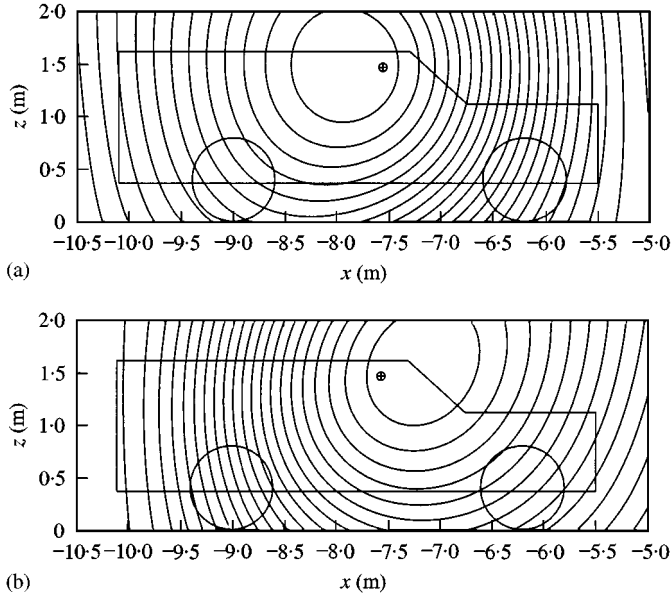

Figure 10. Simulation results for a stationary source at 500 Hz. The symbol ⊕ indicates the source position. (a) Vehicle at the left end of the test section; (b) vehicle at the right end of the test section.

destructive interference, thus yielding incorrectly large amplitudes at those grid points. In fact, the estimated amplitudes can be larger than the estimated amplitude at the actual source location. This tendency becomes more apparent as the source frequency is lowered (see Figure 9). During vehicle passby tests, the maximum oblique look-angles occur when a vehicle is either at the left or the right end of the test section (i.e., at $x = -10$ or 10 m).

Figure 10 shows a simulated source strength distribution over the reconstruction plane obtained by using the new weighting factor when the vehicle was assumed to be positioned at these extreme locations. This simulation was performed using the same 16-microphone array that was used in the passby test experiments; the details of that array will be discussed later. The location of th simulated source radiating a 500 Hz pure tone is indicated by the symbol ⊕ in Figure 10. The source position discrepancies were less than 0·5 m in both cases; however, the apparent shift of source location could be worse for frequencies lower than 500 Hz. Note that the simulated source strength distributions need not be symmetric even though the source was positioned each time symmetrically with respect to the y-axis, since the array configuration used is not symmetric about the y-axis.

4. ARRAY DESIGN

In this section, the array used in the experiments discussed below is described. The microphone array was positioned vertically in a plane parallel to the line of vehicle motion. It was initially decided that the complete array should be 4 m in width and 2 m in height. The total area was divided into three parts vertically and horizontally to form nine subsections (see Figure 11). One microphone was placed at the center of the array at the standard passby microphone height of 1·2 m. The other microphones were randomly positioned within the nine sections, subject to the condition that there should be three

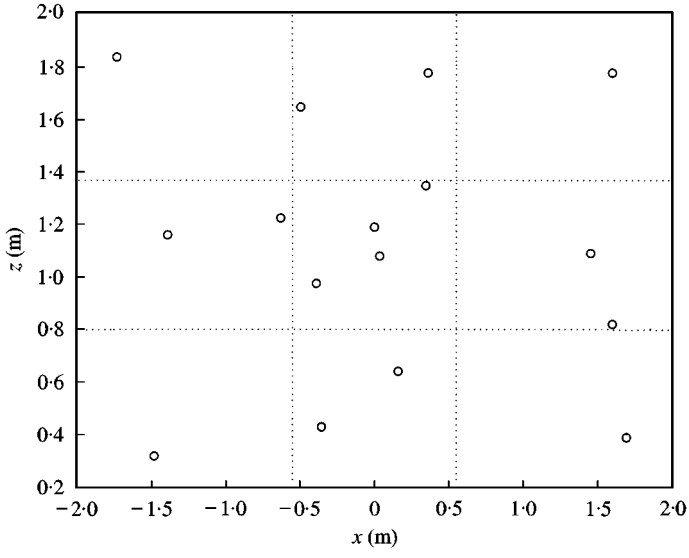

Figure 11. Positions of microphones used in the random array.

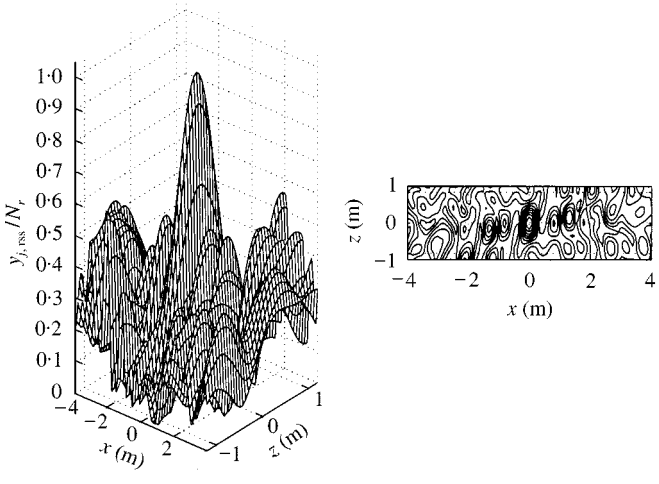

Figure 12. Array pattern at 2000 Hz for the random array used in experimentation.

additional microphones in the center section, two each in the section above, below, left, and right of the center section, and one in each of the corner sections. When the positions of the array elements were determined, there were then "snapped" to the closest grid point based on a spacing of 0·20 m. This numerical procedure was repeated until the array pattern and sidelobe behavior were considered to be acceptable [11].

By requiring the sensor positions to lie on an underlying grid, and by partitioning the array as described, the possibility of the sensors "clumping" in one region of the array was eliminated. The final array design used here is shown in Figure 11, and the array pattern for a monopole source placed at the center of a stationary reconstruction plane 6·5 m directly in front of the receiver array, and operated at 2000 Hz, is displayed in Figure 12. Note that the quantity plotted in Figure 12 is a sound pressure amplitude normalized with respect to the

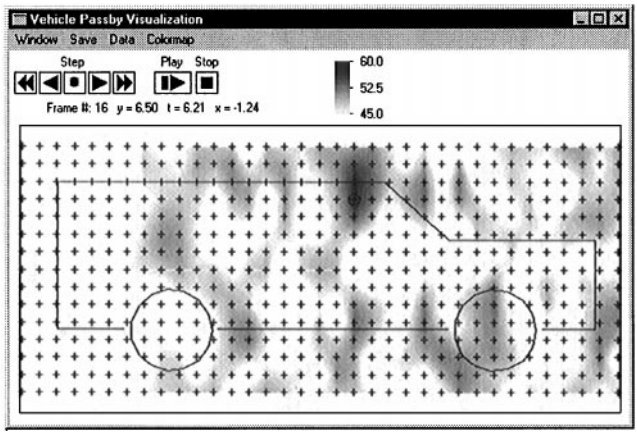

Figure 13. Simulated results for source localization using "backward propagation" for 35 km/h Cruise test. ⊕ denotes simulated loudspeaker location; loudspeaker at 2950 Hz, front hub at $x = -1{\cdot}24$ m, 50 Hz analysis bandwidth.

maximum value (the sound pressure amplitude at the source location). A more complete description of the array design procedure is given in reference [14].

5. RESULTS AND DISCUSSION

5.1. SIMULATION RESULTS

In this subsection, simulated results from both the backward and the forward propagation procedures are presented and compared. In the simulation, source signals were restored on 35×15 evenly spaced grid points on the reconstruction plane: the points were spaced at 15 cm intervals in both the x and z directions. A comparison between the two two different restoration procedures showed that the calculation time was reduced by a factor of there by using the forward propagation procedure when compared to the backward propagation procedure. At the same time, the two procedures produced similar graphical results when applied to a simulated passby test in which a monopole source radiating a 2950 Hz pure tone was positioned to represent a loudspeaker attached to the side of the vehicle: see Figures 13 and 14 for the reconstruction results. It was concluded that the small amount of noise introduced by the linear interpolation process was justified by the significant reduction in computation time, and the forward propagation approach was followed in the remainder of the work discussed here.

5.2. EXPERIMENTAL RESULTS

A measurement of a vehicle passby was conducted using the procedures described in this article. The complete experimental arrangement is shown in schematic form in Figure 15. In the test reported here, the vehicle approached the test section at a constant speed of 58 km/h and then full throttle was applied through the test section. A PC-based data-acquisition system was used to record each of the 16 microphone signals (along with the radar signal and the output of a photocell that was used to establish the absolute position of the vehicle). A total of 8 s of data was acquired at a sample rate of 8192 Hz. The anti-aliasing filters were set at a cut-off frequency of 3200 Hz.

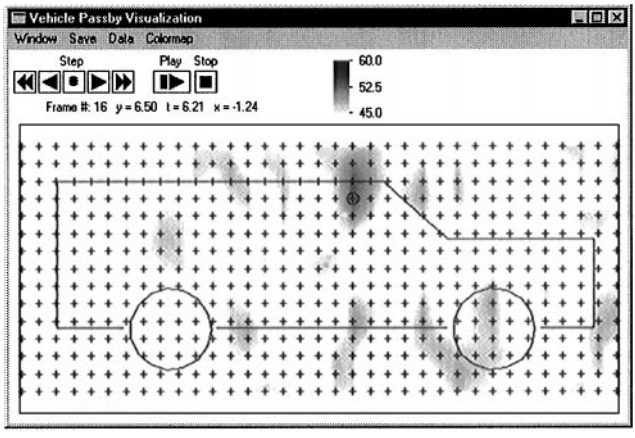

Figure 14. Simulated results for source localization using "forward propagation" for 35 km/h Cruise test. ⊕ denotes simulated loudspeaker location; loudspeaker at 2950 Hz, front hub at $x = -1{\cdot}24$ m, 50 Hz analysis bandwidth.

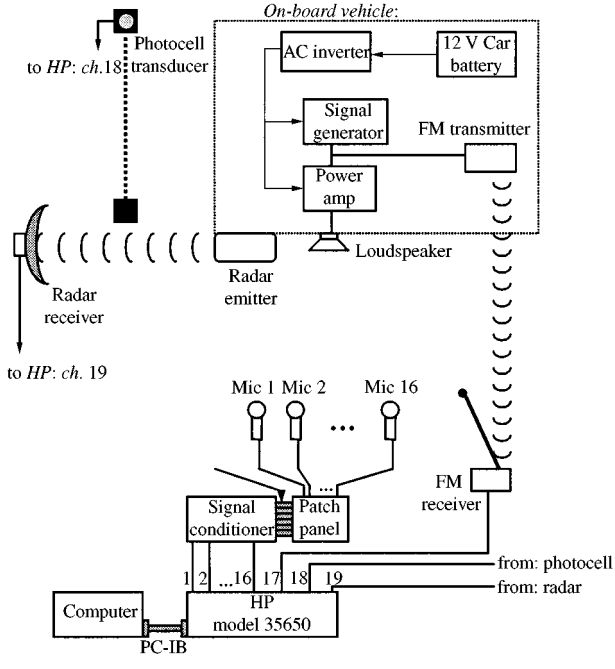

Figure 15. Experimental setup for data acquisition at passby site.

The velocity profile for one of the vehicle passbys, along with the corresponding velocity polynomial, has already been shown in Figure 3. Note that in the curve fit, the velocity polynomial fails to represent the velocity profile once the vehicle begins to slow down after exiting the test section at approximately $t = 5{\cdot}2$ s. When attempting to fit the velocity including the region after the test section, it was found that the added complexity in the velocity trend caused a poor fit through the test section, even when the order of the polynomial was doubled. Since the data beyond the end of the test section was not used in

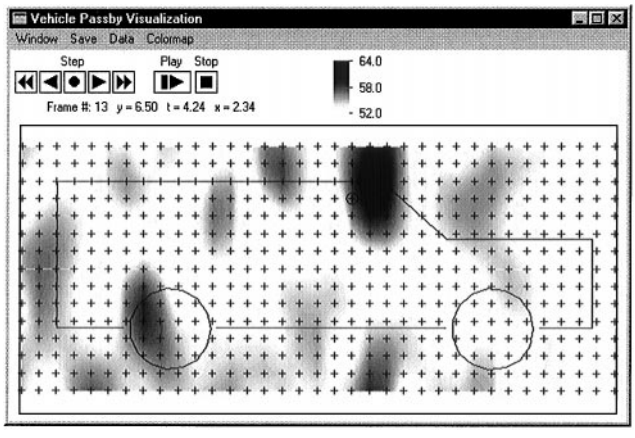

Figure 16. Source localization results for 50 Hz band centered at 1750 Hz (loudspeaker frequency) for acceleration test; ⊕ indicates loudspeaker position.

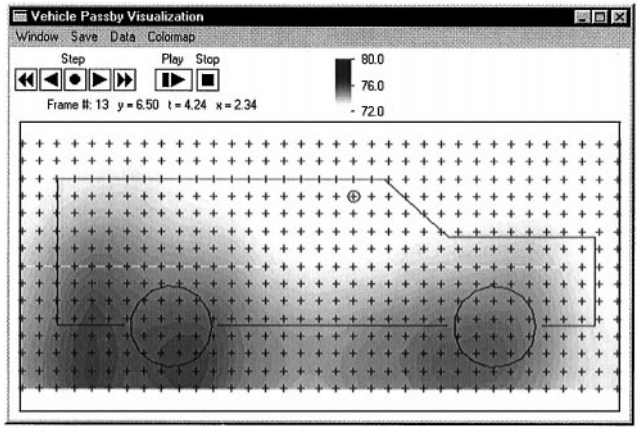

Figure 17. Broadband visualization results for acceleration test; ⊕ indicates loudspeaker position.

the reconstruction, it was determined that ignoring the velocity data beyond the end of the test section would be acceptable.

First, an individual frequency band was examined to check whether the visualization technique could be used to accurately locate the radiation from a loudspeaker mounted on the vehicle. The results for a 50 Hz band centered at 1750 Hz (the loudspeaker frequency) are shown in Figure 16. The results shown correspond to the source distribution when the front wheel hub was 2·34 m in front of the test section centerline. The strongest source strength occurs close to the loudspeaker location as expected. The small discrepancy in the estimation of the loudspeaker location could be ascribed to experimental errors (such as the non-constant distance from the side of the vehicle and the array plane during the test drive). Note that the additional "sources" that appear in this plot probably result from the sidelobes of the array pattern.

The broadband visualization of the sound field radiated during the acceleration test at one moment is shown in Figure 17. It can be seen that in this case the primary noise sources are the two tires, and possibly the exhaust. It is evident that very little noise emanates from

other regions of the vehicle. Note that in this frame, the vehicle is forward of the centerline of the test section, and the tire noise sources appear to be located behind the centerline of the front tire and in front of the tire centerline of the rear tire. This observation is consistent with the observed directivity patterns for tire noise generation, in which the tire radiates more strongly to the front and rear [15].

6. CONCLUSION

The primary goal of present work was to develop a measurement technique that would add a diagnostic capability to standard motor vehicle passby tests. It has been shown here that the representation of the source velocity as a finite order polynomial enables accurate and efficient de-Dopplerization of signals received from sources moving with arbitrary velocity and acceleration. The amplitude correction strategy developed based on a maximum likelihood estimation technique described here makes the present approach different from traditional beamformer methods and allows source strengths and locations to be estimated with reasonable accuracy on an actual vehicle over the usual range of "look" directions encountered in a passby test. However, when the look direction was too oblique (e.g., when the vehicle position was beyond approximately 10 m from the array center), this approach fails to locate the source locations accurately.

In the present work, a random, two-dimensionally sparse array is used to balance the problems of spatial aliasing, angular resolution, and the finite number of available receiver channels. While the use of random arrays can reduce the problem of spatial aliasing, they represent in essence an extreme form of a non-redundant array, and thus sometimes result in undesirably high sidelobe levels. This is why several random array configurations were considered before choosing the one used in the test. It is believed that the use of a sparse, two-dimensional array configuration is a useful approach, but that a systematic method of determining an array configuration of this type in two dimensions has yet to be developed; this is the subject of on-going research.

ACKNOWLEDGMENTS

The authors gratefully acknowledge the financial support of Isuzu Motors Ltd. (contract monitor: Hiroshi Takata). We would also like to thank Gray Penn, former Director of the General Motors Noise and Vibration Center, for making it possible to use the Milford Proving Ground Passby Site, Richard Schumacher for making the necessary arrangements, and Bill Massie and Maurice Evans, for their help with the measurements.

REFERENCES

1. K. D. CHERNE 1993 *Proceedings of the* 1993 *Noise and Vibration Conference*, SAE P-264, 147–152. Motor vehicle noise regulations.
2. G. B. MOEBS, H. KOOK, P. DAVIES and J. S. BOLTON 1998 *Proceedings of Noise-Con* 98, *Ypsilanti, Michigan, April* 5–9, 519–524. The use of two-dimensionally sparse arrays to visualize the sound field radiated by a moving vehicle, with application to motor vehicle passby testing.
3. W. F. KING III and H. J. LETTMANN 1988 *Proceedings of INTER-NOISE* 88, 1391–1396. On locating and identifying sound sources generated by the German 'ICE' train at speeds up to 300 km/h.
4. G. ELIAS 1995 *Proceedings of INTER-NOISE* 95, 1175–1178. Source localization with a two-dimensional focused array: optimal signal processing for a cross-shaped array.

5. M. ABE, J. LIU and K. KIDO 1988 *Proceedings of INTER-NOISE* 88, 159–162. An application of composite complex sinusoidal modeling to the estimation of directions and wave forms of incident plane waves.
6. B. BARSIKOW, W. F. KING III and H. J. LETTMANN 1988 *Proceedings of INTER-NOISE* 88, 167–170. De-Dopplerization of sound radiated by moving sources measured with stationary microphone array.
7. S. DUMBACHER, J. BLOUGH, D. HALLMAN and P. WANG 1995 *Proceedings of the* 1995 *Noise and Vibration Conference*, *SAE P*-291, 1023–1035. Source identification using acoustic array techniques.
8. E. VERTATSCHITSCH and S. HAYKIN 1986 *Proceedings of the IEEE* **74**, 217. Nonredundant arrays.
9. S. BRÜHL and K.-P. SCHMITZ 1993 *Proceedings of INTER-NOISE* 93, 1311–1314. Noise source localization on highspeed trains using different array types.
10. D. H. JOHNSON and D. E. DUDGEON 1993 *Array Signal Processing-Concepts and Techniques*. Englewood Cliffs, NJ: Prentice-Hall.
11. G. B. MOEBS 1997 MSME Thesis, *School of Mechanical Engineering*, *Purdue University*. De-Dopplerization and visualization of sound fields emitted by moving noise sources.
12. G. P. HOWELL, A. J. BRADLEY, M. A. MCCORMICK and J. D. BROWN 1986 *Journal of Sound and Vibration* **105**, 151–167. De-Dopplerization and acoustic imaging of aircraft flyover noise measurements.
13. P. LANCASTER and K. ŠALKAUSKAS 1986 *Curve and Surface Fitting*. London: Academic Press.
14. H. KOOK, P. DAVIES and J. S. BOLTON 1999 *Proceedings of the* 1999 *Noise and Vibration Conference*, *SAE Paper* 99*NV*-227. The design and evaluation of microphone arrays for the visualization of noise sources on moving vehicles.
15. U. SANDBERG and J. A. EJSMONT 1993 *Proceedings of the* 1993 *Noise and Vibration Conference*, *SAE P*-264, 93-111. The art of measuring noise from vehicle tires.